Uranium carbide oxidation from 873 K to 1173 K

Gasparrini, Claudia; Podor, Renaud; Fiquet, Olivier; Horlait, Denis; May, Sarah; Wenman, Mark R.; Lee, William E.

Corrosion Science

DOI:
10.1016/j.corsci.2019.01.044

Published: 01/05/2019

Peer reviewed version

Uranium carbide oxidation from 873 K to 1173 K

Claudia Gasparrini[a], Renaud Podor[b], Olivier Fiquet[c], Denis Horlait[d], Sarah May[e], Mark R. Wenman[a] and William E. Lee[a,f]

[a] Centre for Nuclear Engineering (CNE) & Department of Materials, Imperial College London, South Kensington Campus, London SW7 2AZ, U.K.

[b] Marcoule Institute for Separation Chemistry, ICSM, CEA, CNRS, ENSCM, Montpellier University, Marcoule, France

[c] DEN/DEC/SA3E/LCU Building 315, 13108 Saint Paul lez Durance, Atomic Energy Commission (CEA), Cadarache, France

[d] CNRS/IN2P3 and University of Bordeaux, Centre d'Etudes Nucléaires de Bordeaux-Gradignan, UMR 5797, Chemin du Solarium, 33175 Gradignan, France

[e] National Nuclear Laboratory, Preston Laboratory (A709), Springfields, Salwick, Preston, Lancashire, PR4 0XJ Preston, Lancashire, U.K.

[f] Nuclear Futures Institute, Bangor University, Bangor, LL57 2DG, U.K.

Keywords: Uranium carbide – Uranium oxide – Oxidation – SEM – HT-ESEM – TEM

Abstract

Oxidation of UC was studied from 873 - 1173 K in air and in 10 Pa oxygen using a High Temperature Environmental SEM (HT-ESEM). Conversion to U_3O_8 improved when using 873 K as the oxide product was a fine powder. At higher temperatures (973 K to 1173 K) oxidation slowed due to a densification process with formation of coarse fragments. The oxide fragmentation at 973 K and 1073 K and oxide pulverisation at 873 K were observed *in situ* in a HT-ESEM. Cracking induced fragmentation and pulverisation was linked to stresses generated from the volumetric transformation from UC to U_3O_8.

1 Introduction

There is a significant legacy of so called "*exotic fuels*" and uranics in the UK, which have been stored at Dounreay, Scotland, since the 1950s. The term exotic is used to describe a miscellaneous category of fuels comprising of unirradiated plutonium bearing fuels, unirradiated high enriched uranium fuels and irradiated fuels [1]. Each category comprises of mixed oxides, uranium metal, mixed carbides and uranium tetrafluorides, which were mainly tested in the Prototype Fast Reactor (PFR)[2]. In the uranics

category are some unirradiated uranium carbide (UC) fuels. While the storage conditions on the Dounreay site are secure, the facilities are either being decommissioned or are reaching the end of their life, therefore a longer term storage solution for these fuels is needed. The preferred solution for the unirradiated uranium carbide fuels is to transfer them to the National Nuclear Laboratory (NNL) Preston, Springfields site, UK, for processing into a more stable form[3], better suited for storage. A stable form is needed because UC is pyrophoric[4] in oxygen environment either for long term storage (likely to be in the Capenhurst repository site) or eventual permanent disposal, when a geological disposal facility is available in the UK. Additionally, when in contact with water UC generates flammable gases[5],[6], such as CH_4 and H_2 that need to be minimised in a repository. Oxidation to U_3O_8 is considered the preferable industrial treatment for UC as this can be achieved via oxidation in air. Additionally, U_3O_8 is considered the most preferable oxide for storage as it is inert when compared to UO_2 (as UO_2 oxidises to U_3O_8 via a dramatic volume increase that could potentially damage the container[7]).

The oxidation mechanism of UC is complex and affected by temperature, oxygen partial pressure, morphology of the oxide layer, oxide products, stoichiometry and process conditions[8]. Oxidation of UC was mostly investigated in the 1960s and 1970s when interest of UC as a breeder reactor material was high[9]-[14]. In recent years additional studies were conducted by Berthinier et al.[15], Le Guyadec et al.[16], Siekhaus et al.[17] and Gasparrini et al.[18]. These studies mostly focused on the oxidation mechanism and ignition of UC in a low temperature regime (between 323 K and 848 K) in air or oxygen. Even though many techniques have been used to characterise the products from the oxidation of UC, in particular transmission electron microscopy (TEM)[15],[18] X-ray diffraction[15].[16] and Spectroscopic Ellipsometry[17], the oxidation mechanism of UC is still not entirely understood. This is due to the fact that the products of combustion are multiple, CO, CO_2 and CH_4, and additionally unreacted carbon can be found in form of graphite[15] within UO_2 products. Some of this previous work has assessed the morphology of the oxide via scanning electron microscopy (SEM) showing that a fractured oxide is formed [15], [18], however it has never been shown that the fracture mechanism of the oxide could have a direct effect on the rate of oxidation. The study presented in this work shows that the fracture mechanism of the oxide is key as it affects the rate of reaction and consequently the efficiency of conversion of UC to U_3O_8.

This is the first study reporting on UC oxidation where a thorough characterisation of the cracking and spalling of the oxide is assessed. Previous to this work, Quémard et al.[19] demonstrated that kinetic models postulated so far describing UO_2 oxidation lack of a fundamental understanding of the effects of oxide cracking.

The findings reported in this work have direct application in the industry as recent large scale experimental studies on UC oxidation in the laboratories at NNL Preston, have shown that the oxidation of UC at an industrial level (processing kg at a time) is very challenging at high temperature, 1223 K.

Converting UC to an oxide under controlled conditions in a furnace is difficult as the furnace temperature varies widely as temperature generated from UC ignition can rise rapidly to 2773 K[16]. Additionally, the air flow patterns in the furnace are difficult to control due to the large heat release (the enthalpy of reaction of UC ignition was estimated by Dell & Wheeler to be -1487 kJ/mol[4]) and spikes in temperature during ignition. To achieve high carbide conversion, high temperatures, approximately 1223 K[20], were set in the belt furnace at NNL Preston. However, full conversion of UC to an oxide in one step could not be achieved and unreacted UC was always present in the oxide product. The results reported in this work show that the difficulties encountered in industry when trying to convert large batches of UC at 1223 K were induced by the phenomenon of sintering and densification of the oxide. A low temperature treatment, at 873 K, so far only applied to individual pellets, was found beneficial in terms of conversion and oxide morphology.

This work not only provided a possible solution to an industrial problem, it also provides data for improved modelling of the UC oxidation mechanism. As recently shown by the modelling efforts of Shepherd et al.[21], depending on experimental conditions the oxide produced can be eitherprotective or non-protective [21]. Shepherd et al.[21],[22] assessed the oxidation of UC pellets in air considering the presence of an adherent[21] or non-adherent oxide layer[22]. The presence of an adherent or non-adherent oxide layer was found to affect the reaction rate. The presence of an adherent oxide layer made of U_3O_8, for example, was found to slow down the completion of the reaction from 3.71 h to 3.92 h in a 0.935 cm radius spherical UC sample oxidised in air at 773 K[21]. Shepherd et al.[21] recommended a temperature of 1023 K, in air, for an optimal conversion of UC to an oxide. However, the model proposed[21],[22] did not rely on enough experimental data to justify the choice of considering an adherent or non-adherent oxide layer at the temperature considered. The adherent oxide layer modelled by Shepherd et al.[21], for example, was made of U_3O_8, but usually the adherent oxide layer found on the surface of uranium metal fuels[23] and UC[16] is made of UO_2. U_3O_8 is generally found as a non-adherent powdery layer[24].

Experimental investigations on the nature of the oxide layer formed on UC with temperature are therefore needed to improve the industrial oxidation treatment at NNL and the modelling of its oxidation mechanism. Gathering information on the nature of the oxide, i.e. either UO_2 or U_3O_8, and its thickness, in the case of formation of an adherent oxide layer, would allow better simulation of oxidation reaction rates. Thickness of the oxide layer influences the reaction rates as a thicker adherent oxide layer would increase the time needed for the oxygen to diffuse and reach the interface carbide/oxide[25]. The aim of this work was to provide microstructural information on the nature of the oxide formed on UC fragments and pellets when oxidised in air and oxygen from 873 K to 1173 K. This study was done analysing the products from oxidation in furnaces *ex situ,* and using *in situ* techniques where oxidation was monitored in partial pressures of oxygen as low as 10 Pa. The *in situ* analyses were performed with a high temperature environmental scanning electron microscope (HT-ESEM), at the Marcoule Institute

for the Separation Chemistry (ICSM), France, thanks to a collaboration with the Atomic Energy Commission (CEA) Cadarache who provided UC pellets manufactured several years ago (summer 2013). The experiments performed in furnaces were done at NNL Preston, UK, on aged samples from Dounreay, which were approximately 50 years old. Even though oxidation of UC has previously been reported to be complex and greatly affected by temperature, O_2 partial pressure, reaction products[26] and aging of the material[27], it is shown here that UC oxidation followed similar mechanisms at the same temperature whether performed in 1 atm in air or in 10 Pa O_2. Additionally, similar oxidation behaviour was reported for samples aged 50 years (from Dounreay) and 5 years (manufactured at CEA).

2 Experimental procedure

Three sets of UC samples were used for this study, two sets came from Dounreay and were studied at NNL in the UK with oxidation tests performed in an atmosphere of air in a conventional furnace. One set came from CEA Cadarache and the oxidation studies were done in a HT-ESEM at ICSM in France. The Dounreay pellets were of two types, here called Set A and Set B. Set A comprised of cylindrical pellets with height and diameter of approximately 2 cm, weight of approximately 81 g (these were stored and transported in a box labelled as batch SP 535/A155/I, box 1330 SL) and were stored in air. Set B comprised of annular pellets, height of approximately 1 cm, and an outer and inner diameter of approximately 0.8 cm and 0.2 cm respectively and weight of approximately 5 g. Set A and B, approximately 50 years old, were used for furnace experiments at NNL, see sections 3.1 and 3.2, these were kept in air during storage hence they were considered aged. Set C comprised of UC pellets manufactured at CEA and used for experiments in the HT-ESEM, shown in section 3.3. These were more recently manufactured and characterised at CEA, Cadarache, France and always stored in an inert atmosphere. All three sets of pellets were ^{235}U depleted ($\leq$ 0.3% ^{235}U). Fragments described in section 3.1 were obtained by crushing a pellet from Set A in air in a fume hood. UC pellets were relatively tough, hence the process of crushing with a hammer took several minutes. During crushing and handling of UC in air sparks were visible. Set A comprised UC and a second phase, U_2C_3, which was 5% in weight calculated with Rietveld Analysis from X-Ray Diffraction (XRD). Set A and Set B were used for oxidation experiments in an atmosphere of air using a Carbolite GSM 11/8 muffle furnace (Carbolite Gero Ltd., Hope, UK) with a silica chamber of approximately 125 mm × 185 mm × 345 mm. Prior to insertion in the furnace, samples were weighed and placed in an alumina crucible (Almath Crucibles Ltd., Suffolk, UK), so that the change in weight would not be affected by oxide spallation. All samples were inserted into the furnace at room temperature and removed from the furnace when it was cool or at least when the temperature reached approximately 373 K (quenching could not be performed due to safety issues and cooling usually took several hours). The heating rate was set at 10 K min^{-1}. Experiments on Set A fragments (approximately 1 g) were performed twice using the same conditions and will be referred to as Run 1 and Run 2. Run 1 fragments were oxidised at 873 K, 973 K, 1073 K

and 1173 K for 4 h and at 1173 K for 17 h dwell times (Run 1). Run 2 fragments were oxidised at 873 K, 973 K, 1073 K and 1173 K for 4 h. UC pellets from Set A and Set B were oxidised at 873 K and 1173 K for 6 h dwell time. Dimensions of the remaining unreacted UC pellets were taken with callipers, their mass was measured with a laboratory scale after wiping the surface several times to remove any powder on the surface. UC conversion to an oxide, named *X*, was evaluated with equation 1 where *n* represents the number of UC moles before and after oxidation.

$$X = \frac{n_{t=0} - n_t}{n_{t=0}} \quad (1)$$

UC moles prior to oxidation (at time $t = 0$) are described by $n_{t=0}$, UC moles in the unreacted UC pellets are described by n_t. $n_{t=0}$ is calculated dividing the initial mass of UC with its molecular weight, *M.W.*, (250.04 g mol^{-1}). n_t is calculated dividing the mass of the UC remnant core by its *M.W.*

When the final product was completely oxidised into a powder, equation 1 could not be used as UC was completely converted to U_3O_8. In this case, the pellet conversion was measured by noting the change in weight from the initial UC pellet to the final oxide product. This can be calculated considering a simple mass balance on equation **Error! Reference source not found.**. The expected increase in weight when UC fully converts to U_3O_8 is calculated with equation 2:

$$\Delta w = \left(\frac{M.W._{U_3O_8}}{3 \times \left[\left((0.95 \times M.W._{UC}) + \left(0.05 \times \frac{M.W._{U_2C_3}}{2} \right) \right) \right]} - 1 \right) \times 100 \quad (2)$$

where *w* is the weight and *M.W.* is the molecular weight of either U_3O_8 (842.1 g mol^{-1}), U_2C_3 (512.09 g mol^{-1}) or UC. Equation 2 was formulated considering that the initial UC pellet contained 5 % of U_2C_3 as a second phase. A mass gain of approximately 12 % was found to correspond to complete conversion of UC to U_3O_8.

UC fragments and uranium oxide powders were characterised by XRD using an X'Pert 3 powder diffractometer (PANalytical, The Netherlands) with Ni-filtered CuKα radiation. Scans were performed from 2θ =10 to 75°. Phase identification was performed using the International Centre for Diffraction Data (ICDD) database by comparing peak positions with those listed in the Powder Diffraction Files (PDF 01 073 1709 for UC[28], PDF 01 074 0805 for U_2C_3[29], PDF 00 041 1422 for UO_2[30] all cubic phases, PDF 00 031 1424[31] for U_3O_8). Specific surface area (SSA) measurements was performed by B.E.T on U_3O_8 samples using a Micromeritics Tristar 11 (Micromeritics Instrument Corp.Norcross, GA, USA). Approximately 0.5 g of powder were used in duplicate for each individual run (filling <1/4 of the analysis tube bulb). Samples were first degassed for 1 h at either 373 K and/or 423 K, in vacuum (<20 mTorr) using a Micromeritics VacPrep 061 degasser (Micromeritics Instrument Corp. Norcross,

GA, USA), to remove volatile contaminants. Run 1 samples were all degassed at 423 K. Run 2 samples were first degassed at 373 K, after the analysis was performed samples were reweighed and degassed at 423 K for a second analysis (this was to check the influence of the degassing temperature on the SSA measurements for U_3O_8). Technical grade N_2 was used and calibration was performed with a carbon surface standard. Data were obtained using a Tristar 3000 Micromeritics Surface Area Analyser (Micromeritics Instrument Corp.Norcross, GA, USA) evaluating the amount of N_2 adsorbed at 77 K. SEM characterisation on the oxide powders was performed using a FEI Quanta 200 FEG (Thermo Fisher Scientific, Massachusetts, USA). Carbon analysis on the oxide powders were performed using a EA1108 Fisons (Thermo Fisher Scientific, Massachusetts, USA) (CHNS/O) Analyser Carlo – Erba. Samples were tested three times and the mass used for each measurement was in the range of 2 – 8 mg.

Set C, made of small UC fragments (4-20 mg), was oxidised in a HT-ESEM (FEI Quanta 200 FEG ESEM, Hillsboro, Oregon, US) at ICSM, France. The description of Set C samples and the method for monitoring the sample surface during oxidation can be found in a previous publication[18]. Samples were heated to the desired temperature, between 873 and 1073 K, under vacuum (approximately 6×10^{-3} Pa), only when the set temperature was reached and stabilised (no fluctuations) was an oxygen flux introduced into the ESEM chamber. UC fragments (mass of 6.8, 8.6 and 17.5 mg) were oxidised and monitored *in situ* at 873 K in 10 Pa O_2 and in 50 Pa of air to simulate 10 Pa O_2. UC fragments (mass 9.3 and 10.4 mg) were oxidised at 973 K and 1073 K in 10 Pa O_2. Oxide powders were characterised *ex situ* using a HRTEM, JEOL 2100Plus (JEOL, Tokyo, Japan). Selected Area Diffraction Patterns (SADP) were indexed by matching the d_{hkl} values with PDF reference patterns, (PDF 00 041 1422[30] for UO_2, PDF 00 015 0004[32] for tetragonal U_3O_7 and PDF 01 075 0944[33] for cubic U_4O_9) obtained from the ICDD database. Oxide powders for TEM analysis were prepared by crushing the oxide in pure ethanol with an agate pestle and mortar. Approximately 10 µl of ethanol solution was then deposited on a carbon-coated TEM copper grid.

The influence of volume changes on the oxidation mechanism and on the stresses present in the oxide layer were calculated retrieving crystal structure data from literature[28],[30],[31] and matching these with the compounds analysed by XRD. The percentage volume change, *ΔV(%)*, was calculated using equation 3:

$$\Delta V\ (\%) = 100 \times \left(\frac{\frac{V_{product}}{Z} - \frac{V_{reagent}}{Z}}{\frac{V_{reagent}}{Z}} \right) \quad (3)$$

V is the cell volume and *Z* is the formula per unit cell.

3 Results

Figure 1a is a photograph of a Set A pellet where the outer rim, or outer layer, and the central pellet core are highlighted. Figure 1b shows XRD analysis of fragments taken from the outer layer (which was envisaged to have slowly oxidized during the years of long storage in air) and from the pellet core of Set A pellet (Set B and C did not have an outer rim). XRD showed that both fragments, obtained after crushing the UC pellet in air, were made of UC, U_2C_3 and UO_2 (see Figure 1b), no significant difference was found between the outer layer and the pellet core. The UC and oxide phases present in the samples were identified using PDF 01 073 1709 for UC[28], PDF 01 074 0805 for U_2C_3[29], PDF 00 041 1422 for UO_2[30] all cubic phases, PDF 00 031 1424[31] for U_3O_8. The UO_2 phase may have been present in Set A pellets since their fabrication or formed by slow oxidation during the decades of storage in air atmosphere. The UO_2 and U_2C_3 phases are anyway present only in small quantities compared to UC.

3.1 Fragments oxidised in a furnace

The effect of temperature on the morphology of the oxide products was first monitored on Set A fragments. Runs 1 and 2 showed identical results: at 873 K, the lowest temperature investigated in this study, samples showed a powdery morphology on visual inspection after 4 h (see Figure 2a). On increasing temperature to 1173 K, the oxide was made of coarser fragments recognisable within the powder (see Figure 2d). The transformation of the sample into oxide powder (called here the pulverisation process) at the highest temperature tested, 1173 K, occurred only when the sample was exposed to the oxidising environment for a long time: for 17 h (see Figure 2e).

Secondary electron images (SEIs) revealed that the oxide produced after heat treatment at 1173 K in air for 4 h was made of large rounded particles (particle diameter ranging from 1 to 5 µm, see Figure 2d). These particles had spheroidal equiaxed shape (after 4 h tests) or cuboidal shape (after 17 h test), see SEIs and backscattered electron images (BSEIs) in Figure 2d and e. The oxide formed at 1073 K also showed spherical particles but these were much smaller than those observed at 1173 K (particle diameter ranging from 0.5 to 1 µm, see Figure 2c). Particle sizes of oxide produced at 873 K could not be observed in the SEM as the size was probably too small to be detected with the magnification used (a few particles observed with a diameter < 0.2 µm, see Figure 2a). Both Run 1 and Run 2 powders oxidised at 1173 K for 4 h consisted of spheroidal particles, showing necking between them. Necking is commonly ascribed to sintering processes. Despite the absence of a pressing force, the oxide looked compacted and partially sintered. Particle sizes increase with temperature as shown by the SEIs and BSEIs shown in Figure 2c, d and e. B.E.T. analysis performed on Run 1 and Run 2 samples showed that SSA decreased with increasing temperature (from 873 K to 1173 K) and time (from 4 h to 17 h),

see Figure 3a. Samples oxidised at 873 K had a SSA of 0.57 ± 0.04 m^2 g^{-1}which decreased to 0.18 ± 0.03 m^2 $g^{-1}$for samples oxidised at 1173 K for 4 h. By increasing oxidation time from 4 h to 17 h at 1173 K SSA further decreased to 0.14 ± 0.01 m^2 g^{-1}. Previous studies performed on UO_2 pellets oxidised in air showed similar results as the particle size of U_3O_8 powder formed increased with oxidation temperature[34]. An increase in particle size with temperature was also observed on different parts of the oxide where particles assumed a columnar morphology instead of spherical, see SEIs in Figure 3b, c and d for samples oxidised at 973 K, 1073 K and 1173 K. Columnar oxide has been reported by Song & Yang[35] during oxidation of UO_2 at 1173 K for 0.5 to 4 h in air in a muffle furnace.

The oxide powders shown in Figure 2 and Figure 3, from Run 1 and 2, were examined by XRD. The oxides were comprised of U_3O_8, see Figure 4a and b.

3.2 Pellets oxidised in a furnace

Oxidation of pellets from Set A and B were used to assess UC conversion with temperature. The oxide produced at 1173 K appeared dense due to a sintering process (see Figure 2d), while the oxide produced at 873 K was a powder (see Figure 2a).

The initial pellet dimensions and the conditions they were exposed to in the furnace are summarised in Table 1. Figure 5 shows the pellets before and after oxidation. The temperatures 873 K and 1173 K were chosen because 1173 K was the temperature generally used in the industrial treatment, while 873 K proved to be sufficient to reach complete oxidation of fragments (see section 3.1). After a dwell time of 6 h Set A pellets did not oxidise completely as an unreacted UC core was found underneath the oxide product (an image of the remaining UC core after oxidation is shown in Figure 5a and c). Set B pellets, on the other hand, were fully rendered into a powder. The oxide products from oxidation at 873 K were observed as a uniform dispersed powder (see BSEIs in Figure 5a and b). The oxide products from oxidation at 1173 K were, instead, found as agglomerates (see BSEIs in Figure 5c and d), at higher magnification the oxide particles were rounded and interconnected (see SEI in Figure 5d) as previously observed at the same oxidation temperature on fragments (Figure 2d). Visual inspection indicated the oxide layers formed on Set A pellets, at 1173 K, were thicker and bulkier than those formed at 873 K, which resembled fine detached layers (see images in Figure 5a and c). By evaluating the mass of the unreacted UC cores it was possible to carry out a *quantitative* evaluation of oxide conversion at 873 K and 1173 K on Set A pellets. Table 2 summarises the dimensions and weights of the unreacted UC cores, the weights of the oxide powder from Set B oxidations, oxide conversion, termed *X*, and the carbon content analyses performed on Set A and B oxide layers. Conversion was calculated using equation 1, the pellet oxidised at 873 K showed an oxide conversion of 76%, while the pellet oxidised at 1173 K showed an oxide conversion of 73%. Given that the heat treatment at 1173 K, which resulted

in a 73% conversion, lasted 22 h in total (as quenching could not be allowed for safety reasons, pellets were kept in the furnace during the heating and cooling stages) while the one at 873 K, which resulted in a 76% conversion, lasted 17.5 h, it can be concluded that lowering the oxidation temperature by 300 K is shown to be not only as effective but even more efficient (see Table 1).

Pellets from Set B were fully oxidised as shown in Table 2, a 100% conversion corresponded to a calculated 12% change in mass between the initial carbide sample and oxide products using equation 2. This is in agreement with XRD analyses performed on the oxide powders for all samples shown in Figure 5: all of them matched with U_3O_8 only. Carbon analyses performed on the oxide (see Table 2) showed that even though all oxide products were identified as U_3O_8 by XRD, the oxide from Set A pellets contained 10 times the amount of unreacted carbon compared to Set B pellets. This difference may be associated with either the fact that Set A pellets were not fully converted (only reaching approximately 73% and 76% conversion, hence, particles from the unreacted UC might have been present in the oxide powder) or due to the different type of pellets (cylindrical versus annular). The analysis used to determine carbon content cannot differentiate between elemental carbon and bonded carbon, hence a definitive answer on whether the oxide product contained unreacted carbon or unreacted carbide cannot be evaluated as the XRD could not detect either of these two phases. The difficulties in detecting the residual carbon via XRD may be associated with the fact that the quantity is too low (below detection limits) and it is present together with high Z uranium atoms[36], or to the fact that carbon is amorphous and/or present in nanodomains.

3.3 Fragments oxidised in a HT-ESEM

Furnace experiments on fragments and pellets showed the oxide to partially sinter from 973 K to 1173 K. The start of the sintering process was observed under SEM investigation as the oxide showed neck growth between equiaxed particles (see Figure 2d) along with the presence of columnar grains (see Figure 3b, c and d). Columnar grains are typically found during oxidation of metals[37],[38] or during solidification processes[39] and were previously reported by Song & Yang[35] during oxidation of UO_2.Oxide conversion was found to be reduced by 3 % at 1173 K compared to the lowest temperature studied, 873 K. The decreased conversion may therefore be related to formation of a sintered oxide layer that slowed further oxidation. The oxide formed at high temperature, 1173 K, was identified as U_3O_8 by XRD and the same phase was identified on the low temperature oxide, 873 K. U_3O_8 is, however, usually considered a detachable powder, poorly sinterable at these temperatures. To observe the morphology changes on the oxide with temperature during heating an *in situ* technique was used.

UC fragments inserted in the HT-ESEM chamber readily oxidised when exposed to an oxygen atmosphere, the corners and edges were monitored to follow the surface morphological changes.

Fragments were oxidised at 873 K, the temperature found to improve oxide conversion and render the U_3O_8 oxide in a powder form. Other UC fragments were exposed to higher temperatures, 973 K and 1073 K at the same oxygen partial pressure to compare the effect of temperature on oxide morphology. Figure 6 summarises the findings on fragments oxidised at 873 K, 973 K and 1073 K in a 10 Pa oxygen partial pressure. For all temperatures, as soon as oxygen was inserted into the chamber the sample edges cracked and spallation or exfoliation of small particles occurred. After ~2 minutes from oxygen insertion, what is normally referred to as a "popcorn morphology" of the oxide[40], [41] appeared mostly along sample edges (see Figure 6a to e). In samples oxidised at 873 K, the morphology of the oxide resembling U_3O_8 homogeneously appeared on the entire surface within 5 minutes of oxygen exposure (see Figure 6a, b and c). Within 20 minutes of oxygen exposure samples oxidised at 873 K did not move: they were thus considered fully oxidised at this stage. The behaviour of samples exposed to air or oxygen at the same oxygen partial pressure were similar, showing that oxidation performed in a few tens Pa oxygen can be compared with oxidation in air.

The typical "popcorn" morphology of U_3O_8 homogeneously covered the entire surface of samples oxidised at 873 K within 5 minutes of oxygen exposure, while in samples oxidised at 973 K and 1073 K (see Figure 6d and e) a similar morphology was only observed at the edges and on cracked surfaces after 10 minutes of oxygen exposure. Even after 20 minutes of oxygen exposure, the top sample surface remained visible and the "popcorn" morphology of U_3O_8 preferentially occurred on the new surface formed after sample cracking. Oxidation completed after approximately 1 h at 973 K, while for the sample oxidised at 1073 K the reaction was not complete even after 2 h of exposure. Like the oxide produced from furnace oxidation (see sections 3.1 and 3.2), the oxide produced in HT-ESEM oxidations showed a particle size increase with temperature increase. The oxide particles were larger after treatment at 973 K than after treatment at 873 K (see Figure 7c and a respectively). HRTEM was used to characterise the products from oxidation, the SAD patterns obtained from samples oxidised at 873 K and 973 K are shown in Figure 7b and d. They could both be identified either as polycrystalline cubic UO_2 (PDF 00 041 1422[30]), tetragonal U_3O_7 (PDF 00 015 0004[32]) or cubic U_4O_9 (PDF 01 075 0944[33]). A summary of the *d* spacings calculated from the rings obtained in the SADPs of samples oxidised at 873 K and 973 K is given in Table 3. As is well known, diffraction patterns from these uranium oxide compounds are similar due to the fact that UO_2 can incorporate extra oxygen atoms in its *fcc* cubic fluorite-type structure[42] with minimal distortions. Even though it was not possible to exactly identify the compound formed, apart from being either UO_2 or UO_{2+x}, it is remarkable that no reflections of the higher oxide, U_3O_8, were found. The typical "popcorn-like" morphology of U_3O_8 formed during oxidation of UO_2 in a HT-ESEM[19], was here observed during oxidation from UC to UO_{2+x}. The reasons for this behaviour may be related to the fact that 10 Pa O_2 was not sufficient for UO_{2+x} to undergo complete oxidation to U_3O_8 or that longer times would have been needed to finish the UO_2 conversion to U_3O_8. Still, the oxide morphology at the end of the heat treatment and the crack

formation during oxidation were similar to those observed in the work of Quemard et al.[19] on oxidation of UO_2 to U_3O_8 in a HT-ESEM in an oxygen partial pressure of 265 Pa. To better understand the connection between oxide morphology (popcorn-like) and phase formed (UO_2 instead of U_3O_8), the stresses involved in the change in volume from UC to UO_2 were considered. Usually, the popcorn-like morphology of U_3O_8 is associated with stresses arising from the 36% volume increase during conversion from UO_2[41],[43]. When calculating the volume changes involved in the transformation from UC to UO_2 and from UO_2 to U_3O_8 using equation 3, it is clear that these two transformations are comparable. In particular, the transformation from UC to UO_2 undergoes a considerable volume expansion, 35%, which is only 1% lower than the one calculated from UO_2 to U_3O_8. Hence, the popcorn-like morphology of the oxide observed at 873 K, 973 K and 1073 K during HT-ESEM experiments in Figure 6 and 7 could be associated with the significant volume expansion induced by the transformation from UC to UO_2.

3.4 Stresses involved during oxidation

The volumetric stresses involved in the transformation from UC to U_3O_8 are significant, however, to better explain the exfoliation process on samples at the beginning of the oxidation (see Figure 6a, b, c, d, and e: 2 minutes after oxygen insertion) and the fragmentation process (oxide cracks producing fragments) of samples exposed to 973 K and 1073 K (see Figure 6d and e), the stresses between the carbide and oxide layer were estimated. Cracks were observed to initiate the pulverisation process at 973 K and 1073 K, as the "popcorn-like" morphology developed only on newly cracked surfaces. Cracks on the oxide could either be ascribed to a thermal expansion coefficient mismatch with the carbide or to a mismatch between crystal structures. Measuring stresses between UC and the newly-formed oxide is quite complex (no *in situ* XRD data or neutron diffraction data were available during oxidation), so only a rough estimate of the stresses present in the oxide layer could be performed. An ideal system was considered where the oxide is sitting on top of the carbide layer and the structures of the carbide and oxide were considered isotropic. A simplified isotropic and hydrostatic stress was calculated using the model of Wang et al.[44] via equation 4:

$$\sigma = \frac{E}{1-2\nu}\varepsilon \tag{4}$$

where E is Young's modulus, ν is the Poisson ratio and ε is an averaged strain along all directions. An average isotropic strain in the oxide growing on top of the carbide was calculated using equation 5:

$$\varepsilon_{hkl} = \frac{d-d_0}{d_0} = \frac{\sqrt[3]{V}-\sqrt[3]{V_0}}{\sqrt[3]{V_0}} \tag{5}$$

where d and d_0 are the approximated cubic lattice spacing of the stressed and stress-free material along one particular [hkl] direction, calculated from the retrieved XRD volume cell. As no lattice spacing during oxidation could be measured on UC fragments, the lattice spacing of the stressed oxide layer, d in equation 5, was constrained to match the UC lattice spacing. The stress-free oxide layer, d_0 in equation 5, was taken from the tabulated values of the oxide (free from constraints). The calculated values of the stresses in the oxide layer are given in Table 4. These values are approximate as the system considered was isotropic and the growing oxide layer was constrained on the UC crystal structure. Even though several necessary approximations were used, the stresses evaluated in Table 4, 34 - 52 GPa for UC oxidation to UO_2 and 52 GPa for UO_2 oxidation to U_3O_8, are on the same order of magnitude with stresses previously calculated on oxidation of UO_2 pellets by Ahn[45] and by Szpunar et al.[46]. Ahn[45] reported that a stress of 43.63 GPa for oxidation from UO_2 to U_3O_8 is above the fracture strength value for UO_2, which has been reported to be between 16 and 42 MPa by Ahn[45] and between 50 and 250 MPa by Salvo et al.[47]. Hence, the stress generated during the volume expansion from UO_2 to U_3O_8 appears to be sufficient to cause the oxide to fracture.

Small fragments were observed originating from the outer layer of the samples just after oxygen insertion, then cracking of samples was observed on samples oxidised at 973 K and 1073 K. A behaviour similar to the one observed in this study, like initial fragmentation producing very small fragments followed by a second fragmentation involving large fragments has been previously reported for combustion of carbon materials, like coal[48],[49]. Senneca et al.[48], for example, described a primary fragmentation to be correlated with the formation of small fragments on the outer shell as a consequence of thermal stresses. Large fragments were instead said to originate from core fragmentation due to internal stresses produced by volatilisation[48]. In the case of UC oxidation, the stresses inducing sample fragmentation are considered here to be related with volumetric stresses induced by formation of an oxide and not by thermal stresses. This was observed *in situ* on a UC sample oxidised in 10 Pa O_2 from room temperature to 623 K with heating rate of 20 K min^{-1} followed by heating to 723 K at 1 K min^{-1}. The UC sample (see Figure 8a) did not show signs of volumetric expansion or visible cracking during heating until the first signs of oxidation became visible (particles sat on the surface oxidised) at around 644 K (see Figure 8d). At this stage cracks developed along with a significant volumetric expansion.

4 Discussion

Both oxidation of UC performed *in situ* in a low oxygen atmosphere (10 Pa partial pressure) and in furnaces in air showed that at 873 K oxidation proceeded more quickly and the product was a powder. Oxidation performed at 873 K produced powders with higher SSA (0.57 ± 0.04 m^2 g^{-1}) while oxidation at 973 K and 1073 K produced fragments or powders with smaller SSA (0.18 ± 0.03 m^2 g^{-1} at 1173 K).

Moreover, conversion of UC pellets to U_3O_8 was more efficient at 873 K than at 1173 K. One of the reasons for a slower oxidation at high temperature (1173 K) could be related to the formation of a thick and compact oxide layer (see Figure 2d and Figure 5c). The thickening of the oxide scale observed at 1173 K could be explained by the increase in plasticity of U_3O_8 previously observed at this temperature by Peakall & Antill[25] on UO_2. Peakall & Antill[25] reported thicker oxide layer when oxidation of UO_2 pellets in air was performed at high temperatures (1173-1273 K) instead of low temperatures (623-873 K). An increase in plasticity of the oxide with temperature allows the oxide to accommodate the stresses via deformation rather than cracking. As observed in this work the oxide densifies, partially sinters, delaying cracking at high temperatures (973 K – 1173 K). Partial sintering was shown in Figure 2c, d and e on samples heated at 1073 K and 1173 K; delayed cracking inducing fragments, a phenomenon here called fragmentation, was shown *ex situ* in Figure 5 c and d for samples heated at 1173 K and *in situ* in Figure 6d and e at 973 K and 1073 K. On the contrary, at 873 K the oxide pulverised as soon as oxygen was inserted in the atmosphere, this can be observed in Figure 6a, b and c. The phenomenon here called pulverisation (formation of fine powder) was observed on samples heated at 873 K and it was shown *ex situ* in Figure 5a and b and *in situ* in Figure 5a, b and c. This phenomenon can be explained by the fact that the oxide at this temperature cannot accommodate the stresses via deformation, hence, it cracks. The word pulverisation was chosen because the oxide under visual inspection resembles a fine powder, as no large fragments can be seen. This is confirmed by B.E.T. analysis (see Figure 3a) where samples oxidised at 873 K have a larger SSA to the ones oxidised at 1173 K(SSA decreased from about 0.6 $m^2g^{-1}$to 0.2 $m^2 g^{-1}$ with increasing temperature). The presence of important stresses in the oxide layer are known to be substantial as shown in Table 4. The formation of a dense oxide layer (at 1173 K) instead of a cracked one (at 873 K) would therefore slow the diffusion of oxygen through the oxide layer and reduce the available surface area for the reaction to occur. HT-ESEM experiments enabled the surface morphological changes of UC samples to be monitored and confirmed the results obtained on UC pellets and fragments oxidised in a furnace in air. Oxidation at 873 K occurred more rapidly than oxidation at 973 K and 1073 K, samples at 873 K pulverised while samples at 973 K and 1073 K fragmented before pulverisation occurred. Samples oxidised at 873 K pulverised homogeneously and oxidation was completed within 20 minutes in the HT-ESEM. Samples oxidised at 973 K and 1073 K, instead, only pulverised around the edges and on freshly cracked surfaces. Cracks were observed across the sample while the top surface remained visible with no or little change detectable (see Figure 6d and e). The product from furnace experiments in air was U_3O_8, while HT-ESEM experiments produced UO_2 or UO_{2+x} due to the reduced oxygen partial pressure available. However, in both cases temperature influenced the oxide products morphology in the same way and the time needed to reach complete oxidation. Temperature was a key parameter for control of the oxide product characteristics. The influence of mechanical stresses on oxidation with temperature has been studied in silicon nitride based ceramics [50] and similar findings were reported but in a different temperature range. In the case of reaction-bonded silicon nitride, below 1273 K the oxide was

considered brittle and cracked as the plasticity of the oxide was insufficient to accommodate mechanical stresses arising from volume expansion, between 1273 K and 1573 K, instead, the oxide was found to be ductile.

Even though the final destiny of the U_3O_8 powders produced during oxidation treatment of the Dounreay UC pellets is not clear yet, having a powder with higher SSA, using 873 K treatment, could benefit the sintering process of possible recycled fuels in the future. Previous studies by Yang et al.[40] on oxidation of UO_2 showed that by lowering the temperature from 723 K to 598 K, the U_3O_8 powder produced had higher SSA and smaller particle size (SSA of 1.50 m^2 $g^{-1}$for U_3O_8 powder oxidised at 598 K and SSA of 0.66 m^2 g^{-1} for U_3O_8 powder oxidised at 723 K). Yang et al.[40] observed that a finer U_3O_8 powder was more sinter-active and improved the densification of recycled UO_2 pellets compared to high-temperature (723 K) oxidised U_3O_8 powder[40].

The drawback of using 873 K for UC oxidation was the increase in unreacted carbon in the oxide product, however, the quantities measured remained in the ppm range. The lower concentration of carbon measured in the uranium oxide produced at 1173 K compared to that produced at 873 K could be related to the different oxide product morphology, which may trap carbon nanodomains, or to the increased gasification of unreacted carbon as CO_2. The columnar grain morphology observed on the oxide formed at 1173 K could have had an effect on the escape of CO/CO_2 gas from the oxide. Columnar grains are reported in other systems in conjunction with void migration[51] or bubble migration along steep thermal gradients[52]. In this case the columnar morphology was reported to be a favourable route for vapour-phase transport[52]. The increased ease by which CO/CO_2 could leave the system when the oxide assumes columnar morphology (after oxidation at 973 K, 1073 K and 1173 K, see Figure 3b, c and d) would lead to less carbon dispersed in the oxide layer.

A schematic of the mechanism of UC oxidation is shown in Figure 9. All samples observed under the HT-ESEM underwent pulverisation along the edges and corners as soon as oxygen was inserted (see Figure 6), this process is called exfoliation in Figure 9. The slower oxide conversion observed at 1173 K compared to 873 K was linked with the fragmentation process of the oxide observed *ex situ* on the UC pellets oxidised in a furnace (see Figure 2b, c and d and BSEIs in Figure 5c and d) and *in situ* during oxidation in a HT-ESEM (see Figure 6d and e). The fragmentation process was induced by the ability of the oxide to plastically deform accommodating the stresses related to the volumetric expansion from UC to the oxide before cracking. At 873 K samples pulverised homogeneously with time all over the observable surface (see Figure 6a, b and c), this was related to the inability of the oxide to accommodate volumetric stresses related to oxidation.. Fragmentation occurred on samples exposed to 973 K, 1073 K and 1173 K where a columnar morphology of the oxide was also observed. The hypothesis of the columnar morphology of the oxide facilitating the escape of gases, CO/CO_2, from the system is also

shown in Figure 9, however further analyses should be performed to clarify the escape route for CO/CO_2.

5 Conclusions

UC oxidation studied from 873 K to 1173 K in air and in 10 Pa oxygen atmosphere revealed that:

- Lowering the temperature, from 1173 K to 873 K, in furnace treatments was found beneficial in converting UC pellets to U_3O_8. The benefits in using 873 K when converting UC to an oxide, U_3O_8, were related to an improved oxide conversion (76% at 873 K versus 73% at 1173 K) and to a finer oxide powder. U_3O_8 powder produced at 873 K was made of smaller particles and higher SSA (0.57 ± 0.04 m^2 g^{-1}) compared to the one found at 1173 K (0.18 ± 0.03 m^2 g^{-1}).
- Slower conversion at 1173 K was related to a dense oxide formed of equiaxed particles and columnar grains.
- UC oxidation was influenced by temperature in the same way as in experiments performed in furnaces in 1 atm air and in a HT-ESEM in 10 Pa O_2: notably oxidation at 873 K proceeded more quickly and produced a finer powder.
- Using *in situ* techniques enabled the changes of sample morphology with temperature to be detected. Samples exfoliation (pulverisation along edges and corners as soon as oxygen was inserted) occurred on all samples oxidised from 873 K to 1173 K just after oxygen insertion. Samples oxidised at 873 K pulverised homogeneously all over the surface until oxidation completed. Pulverisation on samples oxidised at 973 K and 1073 K instead only occurred after samples cracked into fragments.
- Cracks and pulverisation observed during oxidation were correlated with the significant stresses involved in the volume change associated with oxide formation on UC (UO_2 formation comes with a 35% volume expansion, subsequent formation of U_3O_8 comes with a 36% volume expansion).

6 Data Availability

The raw data required to reproduce these findings are available upon request to c.gasparrini14@imperial.ac.uk.

7 Acknowledgments and Support

The authors are grateful to the EPSRC DISTINCTIVE (Decommissioning, Immobilisation and Storage soluTIons for NuClear wasTe InVEntories) Consortium for their financial support of this project (EPSRC Industrial Case Award EP/M507428/1 Grant and the DISTINCTIVE EP/ L014041/1 Grant).

We thank Dr Mahmoud Ardakani and Dr Ecaterina Ware for help with TEM analyses performed at the Harvey Flower Electron Microscopy Suite, Department of Materials, Imperial College London. We also thank Simon Everall for performing B.E.T. analyses, Jennifer Alcock for performing carbon analyses and Dr Duncan Coppersthwaite for technical supervision at the National Nuclear Laboratory, building A709, Preston.

8 References

[1] Nuclear Decommissioning Authority, Exotic fuels and nuclear materials - Dounreay - Preferred options (Gate B). Document Reference: SMS/TS/B&C3/NM&EF/001/B, (2013).

[2] Nuclear Decommissioning Authority, Exotic fuels and nuclear materials - Dounreay - Credible options - Final Document Ref SMS/TS/B&C3/NM&EF/001/A, (2012).

[3] Nuclear Decommissioning Authority, Uranics: credible options summary (Gate A). Document reference: SMS/TS/B2-UR/002/A v1.0, (2014) 1–11.

[4] M. Dell, V.J. Wheeler, The ignition of uranium mononitride and uranium monocarbide in oxygen, J. Nucl. Mater. 21 (1966) 328–336.

[5] Y. Hori, T. Mukaibo, Kinetic study of the reaction between uranium monocarbide and water vapor, Bull. Chem. Soc. Jpn. 40 (1967) 1878–1883. doi:10.1246/bcsj.40.1878.

[6] A. Schürenkämper, Kinetic studies of the hydrolysis of uranium monocarbide in the temperature range 30°C–90°C, J. Inorg. Nucl. Chem. 32 (1970) 417–429. doi:10.1016/0022-1902(70)80249-4.

[7] K.O. Kvashnina, S.M. Butorin, P. Martin, P. Glatzel, Chemical state of complex uranium oxides, Phys. Rev. Lett. 111 (2013) 253002. doi:10.1103/PhysRevLett.111.253002.

[8] C. Guéneau, A. Chartier, L. Van Brutzel, Thermodynamic and thermophysical properties of the actinide oxides, in: Sect. 2.02 Compr. Nucl. Mater. - Vol. 2, 2012: pp. 21–60.

[9] A. Van Tets, Reaction of uranium monocarbide powder in oxidizing atmospheres, Thermochim. Acta. 6 (1973) 195–203.

[10] G. Matcheret, L'oxydation des carbures d'uranium par des reactifs gazeux, Commis. à l'Energie At. Report, BIB-183. (1970).

[11] K. Naito, N. Kamegashira, T. Kondo, S. Takeda, Isothermal oxidation of uranium monocarbide powder under controlled oxygen partial pressures, J. Nucl. Sci. Technol. 13 (1976) 260–267. doi:10.1080/18811248.1976.9734020.

[12] T. Ohmichi, T. Honda, The Oxidation of UC and UN Powder in Air, J. Nucl. Sci. Technol. 5 (1968) 600–602. doi:10.1080/18811248.1968.9732521.

[13] K.A. Peakall, J.E. Antill, Oxidation of uranium monocarbide, J. Less-Common Met. 4 (1962) 426–435.

[14] H. Matzke, Effect of humidity on the surface oxidation of UC single crystals at room temperature, J. Appl. Phys. 40 (1969) 3819–3824. doi:10.1063/1.1658277.

[15] C. Berthinier, C. Rado, O. Dugne, M. Cabie, C. Chatillon, R. Boichot, E. Blanquet, Experimental kinetic study of oxidation of uranium monocarbide powders under controlled oxygen partial pressures below 230°C, J. Nucl. Mater. 432 (2013) 505–519. doi:10.1016/j.jnucmat.2012.08.002.

[16] F. Le Guyadec, C. Rado, S. Joffre, S. Coullomb, C. Chatillon, E. Blanquet, Thermodynamic and experimental study of UC powders ignition, J. Nucl. Mater. 393 (2009) 333–342. doi:10.1016/j.jnucmat.2009.06.009.

[17] W.J. Siekhaus, B. Donald, C. Saw, A. Nelson, The optical properties of uranium carbide and its rate of oxidation in air determined by spectroscopic ellipsometry, No. LLNL-CONF-678401. Lawrence Livermore Natl. Lab.(LLNL), Livermore, CA (United States),. (2015).

[18] C. Gasparrini, R. Podor, D. Horlait, M.J.D. Rushton, O. Fiquet, W.E. Lee, Oxidation of UC: an in situ high temperature environmental scanning electron microscopy study, J. Nucl. Mater. 494 (2017) 127–137. doi:10.1016/j.jnucmat.2017.07.016.

[19] L. Quémard, L. Desgranges, V. Bouineau, M. Pijolat, G. Baldinozzi, N. Millot, J.C. Nièpce, A. Poulesquen, On the origin of the sigmoid shape in the UO_2 oxidation weight gain curves, J. Eur. Ceram. Soc. 29 (2009) 2791–2798. doi:10.1016/j.jeurceramsoc.2009.04.010.

[20] D.P. Coppersthwaite, J.T. Semeraz, Uranium Carbide Oxidation . Phase 3 Trials. Nexia Solutions Technical Report, 5884, provided by NNL, 2005.

[21] J.S. Shepherd, M. Fairweather, B.C. Hanson, P.J. Heggs, Mathematical model of the oxidation of a uranium carbide fuel pellet including an adherent product layer, Appl. Math. Model. 45

(2017) 784–801. doi:10.1016/j.apm.2017.01.041.

[22] J.S. Shepherd, M. Fairweather, P.J. Heggs, B.C. Hanson, Mathematical modelling of the pre-oxidation of a uranium carbide fuel pellet, Comput. Chem. Eng. 83 (2015) 203–213. doi:10.1016/j.compchemeng.2015.05.001.

[23] S. Orman, G. Picton, J.C. Ruckman, Uranium oxides formed in air and water in the temperature range 200-375 ^{0}C, Oxid. Met. 1 (1969).

[24] H. Matzke, Science of Advanced LMFBR Fuels : Solid State Physics, Chemistry, and Technology of Carbides, Nitrides, and Carbonitrides of Uranium and Plutonium, North Holland, 1986.

[25] K.A. Peakall, J.E. Antill, Oxidation of uranium dioxide in air at 350–1000°C, J. Nucl. Mater. 2 (1960) 194–195. doi:10.1021/j150566a002.

[26] D. Manara, F. De Bruycker, A.K. Sengupta, R. Agarwal, H.S. Kamath, Thermodynamic and thermophysical properties of the actinide carbides, Elsevier, 2012. doi:10.1016/B978-0-08-056033-5.00011-2.

[27] E.W. Murbach, G.E. Brand, Experiments on pyrochemical reprocessing of uranium carbide fuel, Symp. Reprocess. Nucl. Fuels. Nucl Met, Met. Soc. AIME. 15 (1969) 123–139.

[28] R.E. Rundle, N.C. Baenziger, A.S. Wilson, R.A. McDonald, The structures of the carbides, nitrides and oxides of uranium, J. Am. Chem. Soc. 70 (1948) 99–105.

[29] A.E. Austin, Carbon positions in uranium carbides, Acta Crystallogr. 12 (1959) 159–161. doi:10.1107/S0365110X59000445.

[30] R. Fritsche, C. Sussieck-Fornefeld, ICDD Grant-in-Aid, Min.- Petr. Inst., Univ., Heidelberg, Germany, (1988).

[31] B.O. Loopstra, The phase transition in alpha-U_3O_8 at 210°C, J. Appl. Cryst. 3 (1970) 94–96.

[32] E.F. Westrum, F. Grønvold, Triuranium heptaoxides: Heat capacities and thermodynamic properties of α- and β-U_3O_7 from 5 to 350°K, J. Phys. Chem. Solids. 23 (1962) 39–53. doi:10.1016/0022-3697(62)90055-0.

[33] B. Belbeoch, C. Piekarski, P. Pério, Structure de U_4O_9, Acta Crystallogr. 14 (1961) 837–843. doi:10.1107/S0365110X61002448.

[34] M. Iwasaki, T. Sakurai, N. Ishikawa, Y. Kobayashi, Oxidation of UO_2 pellets in air, J. Nucl. Sci. Technol. 5 (1968) 652–653. doi:10.1080/18811248.1968.9732532.

[35] K.W. Song, M.S. Yang, Formation of columnar U_3O_8 grains on the oxidation of UO_2 pellets in air at 900°C, J. Nucl. Mater. 209 (1994) 270–273. doi:10.1016/0022-3115(94)90262-3.

[36] L. Biasetto, S. Corradetti, S. Carturan, R. Eloirdi, P. Amador-Celdran, D. Staicu, O.D. Blanco, A. Andrighetto, Morphological and functional effects of graphene on the synthesis of uranium carbide for isotopes production targets, Sci. Rep. 8 (2018) 8272. doi:10.1038/s41598-018-26572-5.

[37] S.C. Cifuentes, M. a. Monge, P. Pérez, On the oxidation mechanism of pure tungsten in the temperature range 600-800°C, Corros. Sci. 57 (2012) 114–121. doi:10.1016/j.corsci.2011.12.027.

[38] W. Gong, H. Zhang, Y. Qiao, H. Tian, X. Ni, Z. Li, X. Wang, Grain morphology and crystal structure of pre-transition oxides formed on Zircaloy-4, Corros. Sci. 74 (2013) 323–331. doi:10.1016/j.corsci.2013.05.007.

[39] W. Kurz, C. Bezençon, M. Gäumann, Columnar to equiaxed transition in solidification processing, Sci. Technol. Adv. Mater. 2 (2001) 185–191. doi:10.1016/S1468-6996(01)00047-X.

[40] J.H. Yang, K.W. Kang, K.S. Kim, Y.W. Rhee, K.W. Song, Recycling process for sinter-active U_3O_8 powders, J. Nucl. Sci. Technol. 47 (2010) 538–541. doi:10.1080/18811248.2010.9711976.

[41] R.J. McEachern, P. Taylor, A review of the oxidation of uranium dioxide at temperatures below 400°C, J. Nucl. Mater. 254 (1998) 87–121. doi:10.1016/S0022-3115(97)00343-7.

[42] F. Garrido, R.M. Ibberson, L. Nowicki, B.T.M. Willis, Cuboctahedral oxygen clusters in U_3O_7, J. Nucl. Mater. 322 (2003) 87–89. doi:10.1016/S0022-3115(03)00318-0.

[43] K.W. Song, K.S. Kim, Y.M. Kim, Y.H. Jung, Sintering of mixed UO_2 and U_3O_8 powder compacts, J. Nucl. Mater. 277 (2000) 123–129. doi:10.1016/S0022-3115(99)00212-3.

[44] X.L. Wang, C.R. Hubbard, K.B. Alexander, P.F. Bech, Neutron diffraction measurements of the residual stresses in Al_2O_3-$ZrO_2(CeO_2)$ ceramic composites, J. Am. Ceram. Soc. 77 (1994) 1569–1575.

[45] T.M. Ahn, Dry oxidation and fracture of LWR spent fuels, NUREG-1565, Div. Waste Manag. Off. Nucl. Mater. Saf. Safeguards, U.S. Nucl. Regul. Comm. Washington, DC 20555-0001. (1996).

[46] B. Szpunar, J.A. Szpunar, V. Milman, A. Goldberg, Implication of volume changes in uranium oxides: a density functional study, Solid State Sci. 24 (2013) 44–53. doi:10.1016/j.solidstatesciences.2013.06.013.

[47] M. Salvo, J. Sercombe, T. Helfer, P. Sornay, T. Désoyer, Experimental characterization and modeling of UO_2 grain boundary cracking at high temperatures and high strain rates, J. Nucl. Mater. 460 (2015) 184–199. doi:10.1016/j.jnucmat.2015.02.018.

[48] O. Senneca, F. Scala, R. Chirone, P. Salatino, Relevance of structure, fragmentation and reactivity of coal to combustion and oxy-combustion, Fuel. 201 (2017) 65–80. doi:10.1016/j.fuel.2016.11.034.

[49] O. Senneca, Oxidation of Carbon: What We Know and What We Still Need to Know, Energy Procedia. 120 (2017) 62–74. doi:10.1016/j.egypro.2017.07.155.

[50] G. Grathwohl, F. Porz, Y. Gogotsi, Effect of oxidation on creep of silicon-nitride-based ceramics, in: K.G. Nickel (Ed.), Corros. Adv. Ceram., Springer, 1994: pp. 441–452. doi:10.1007/978-94-011-1182-9.

[51] J.R. MacEwan, V.B. Lawson, Grain growth in sintered uranium dioxide: II, columnar grain growth, J. Am. Ceram. Soc. 45 (1962) 42–46. doi:10.1111/j.1151-2916.1962.tb11027.x.

[52] F.A. Nichols, Transport phenomena in nuclear fuels under severe temperature gradients, J. Nucl. Mater. 84 (1979) 1–25. doi:10.1016/0022-3115(79)90147-8.

[53] S.M. Lang, Properties of high-temperature ceramics and cermets: elasticity and density at room temperature, Monogr. 6, Natl. Bur. Stand. Washingt. D.C. (1960). http://catalog.hathitrust.org/Record/001688033%5Cnhttp://hdl.handle.net/2027/mdp.39015026567951 (no.6-17).

[54] D.L. Hagrman, G.A. Reymann, Matpro — Version 11 A Handbook of Materials Properties for Use in the Analysis of Light Water Reactor Fuel Rod Behavior, Idaho Natl. Eng. Lab., Idaho Falls. (1979) 1–543. papers3://publication/uuid/101F5A42-3961-4276-A1D0-E42D3336EBF9.

[55] B. Szpunar, J.A. Szpunar, V. Milman, A. Goldberg, Implication of volume changes in uranium

oxides: a density functional study, Solid State Sci. 24 (2013) 44–53. doi:10.1016/j.solidstatesciences.2013.06.013.

[56] B. Szpunar, J.A. Szpunar, Theoretical investigation of structural and mechanical properties of uranium oxide, Uranium 2010, Proc. 3rd Int. Conf. Uranium, Saskatoon, Saskatchewan, Canada. 2 (2010) 177–187. doi:10.1016/j.jpcs.2015.10.011.

8.1 List of Figures

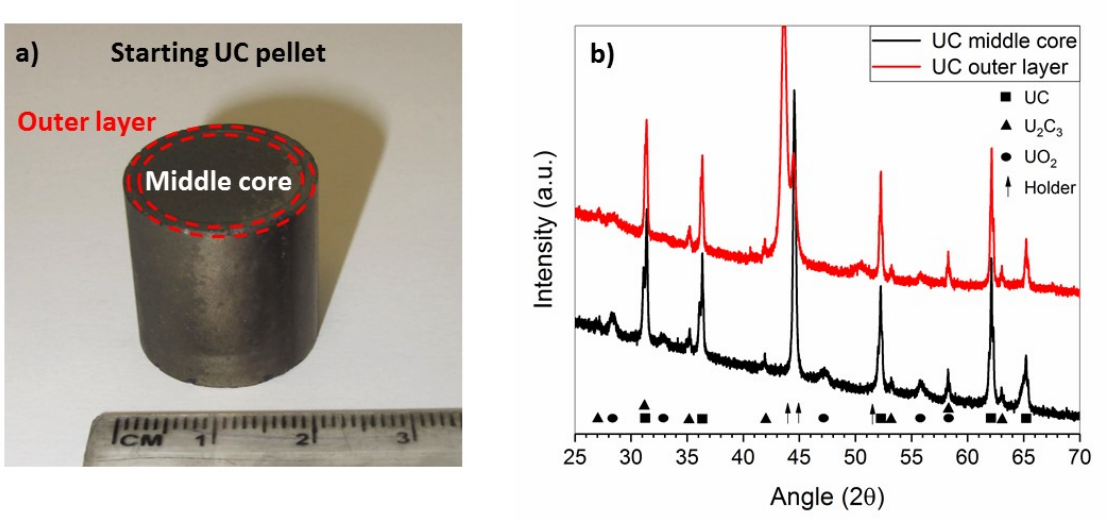

Figure 1 a) Photograph of a cylindrical UC pellet from Set A: the outer layer is highlighted with a red dashed line; b) XRD patterns of fragments taken from the pellet core and the outer layer

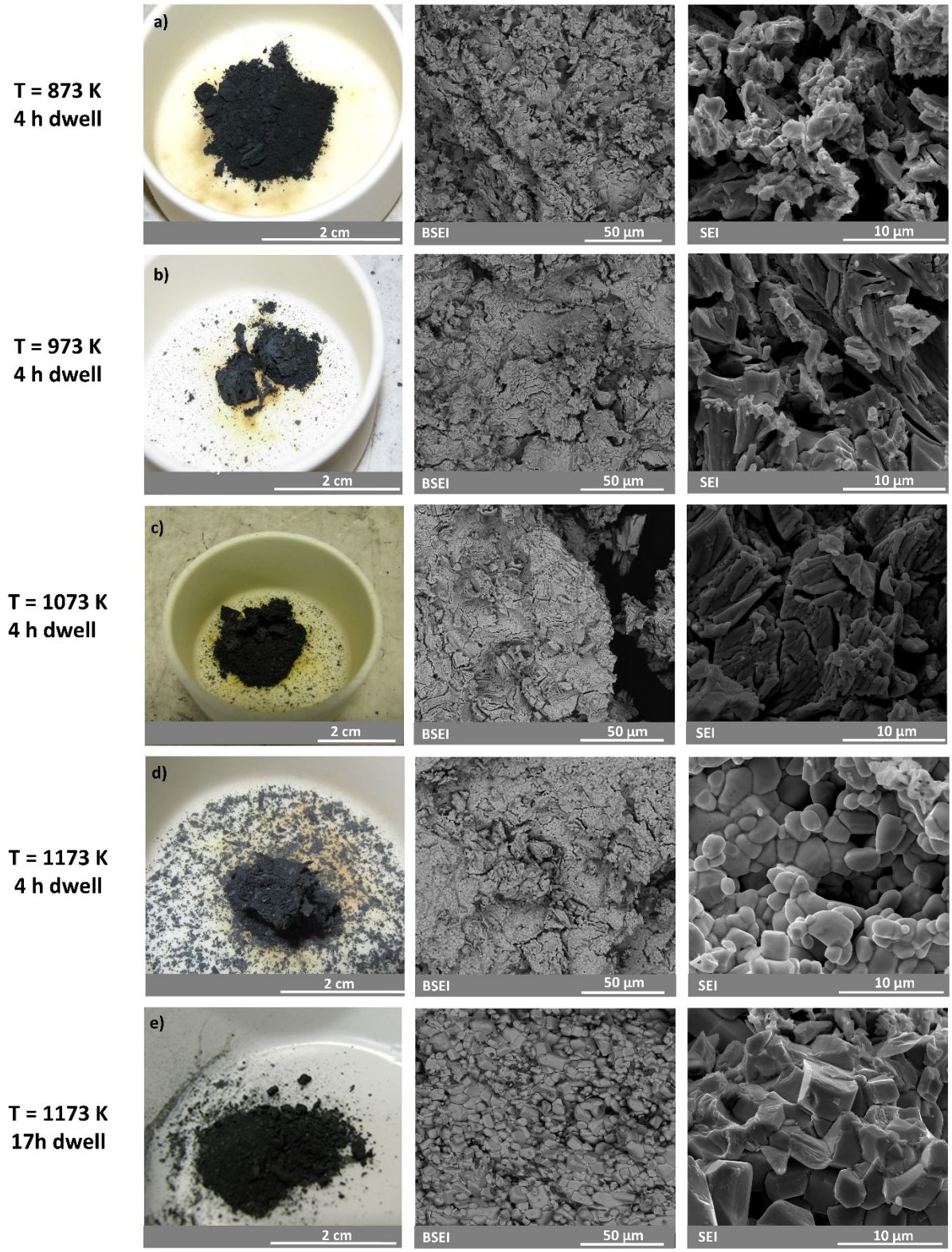

Figure 2 Morphology of the oxide observed on Run 1 samples from Set A fragments. From left to right: photographs, BSEIs and SEIs of fragments oxidised in air at: a) 873 K for 4 h, b) 973 K for 4 h, c) 1073 K for 4 h, d) 1173 K for 4 h and e) 1173 K for 17h.

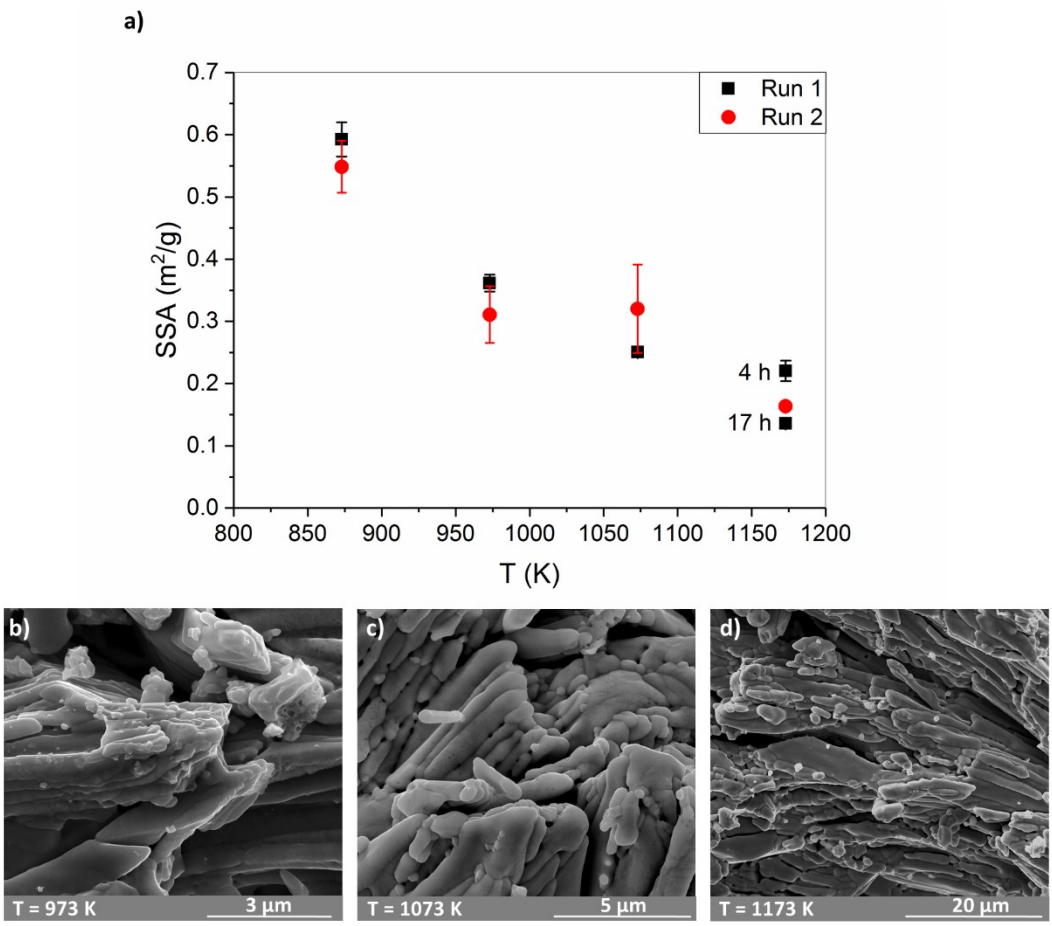

Figure 3 a) B.E.T. analysis of powders from Run 1 and Run 2 after oxidation in air at 873 K, 973 K, 1073 K and 1173 K. SEIs of samples oxidised at 973 K b), 1073 K c), and 1173 K d) for 4 h in air from samples shown in Figure 2 showing a columnar morphology of the oxide.

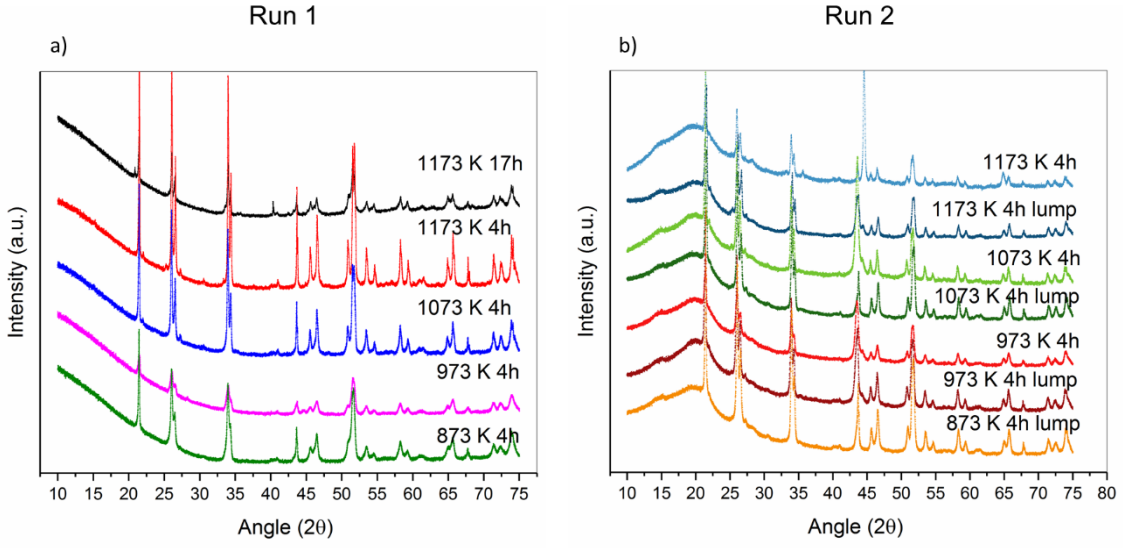

Figure 4 XRD spectra of UC fragments oxidised in air in a muffle furnace: a) Run 1: treatments at 873 K, 973 K, 1073 K, 1173 K for 4 h and at 1173 K for 17 h; b) Run 2: treatments at 873 K, 973 K, 1073 K, 1173 K for 4 h.

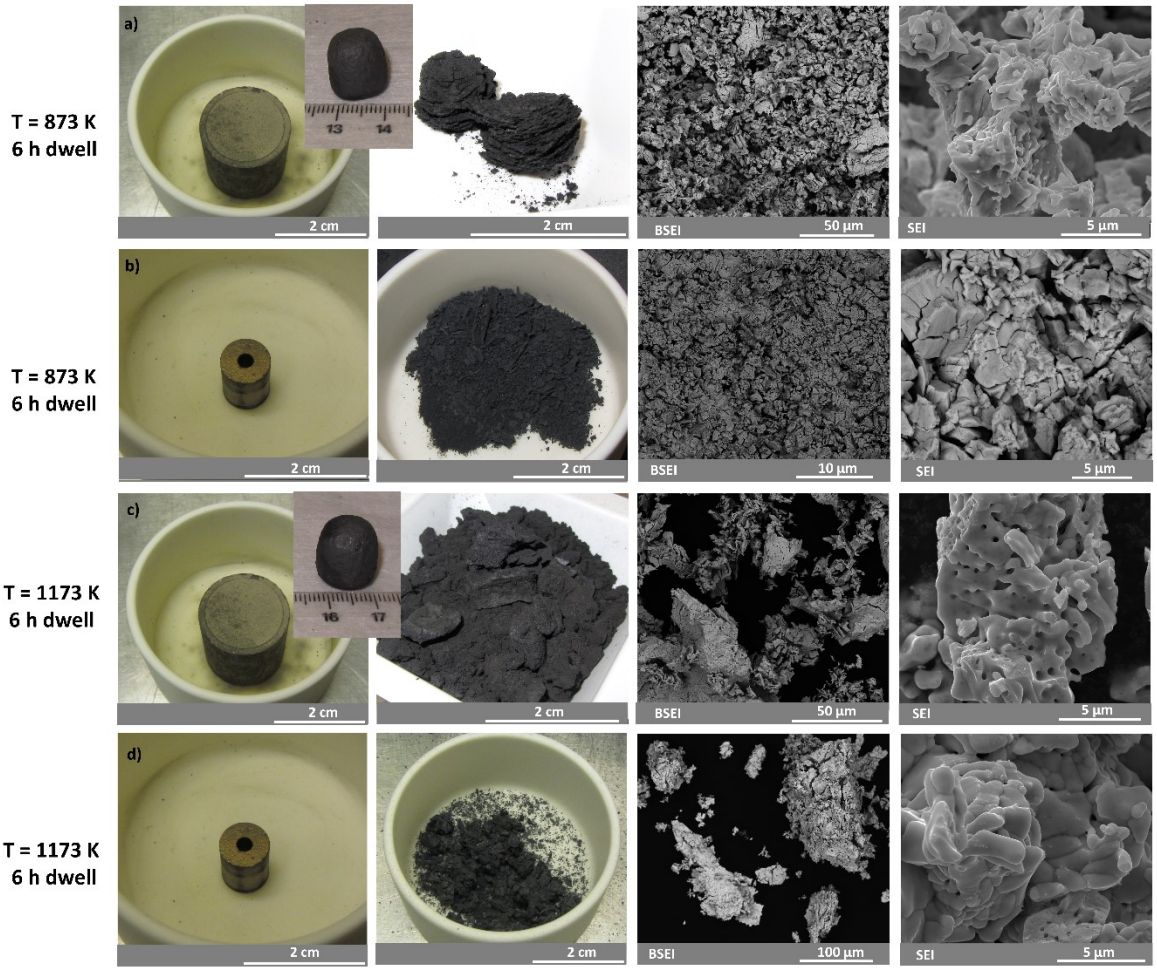

Figure 5 Macroscopic appearance of UC pellets and morphology of the products from oxidation (remaining UC pellet shown in a and c) revealed by photographs, BSEI and SEI respectively for: a) cylindrical pellet oxidised at 873 K for 6 h (sample P3); b) annular pellet oxidised at 873 K for 6 h (sample P4); c) cylindrical pellet oxidised at 1173 K for 6 h (sample P1); d) annular pellet oxidised at 1173 K for 6 h (sample P2). For clarity, the same photographs from a) and b) were used in c) and d) to represent the initial stage of the pellet.

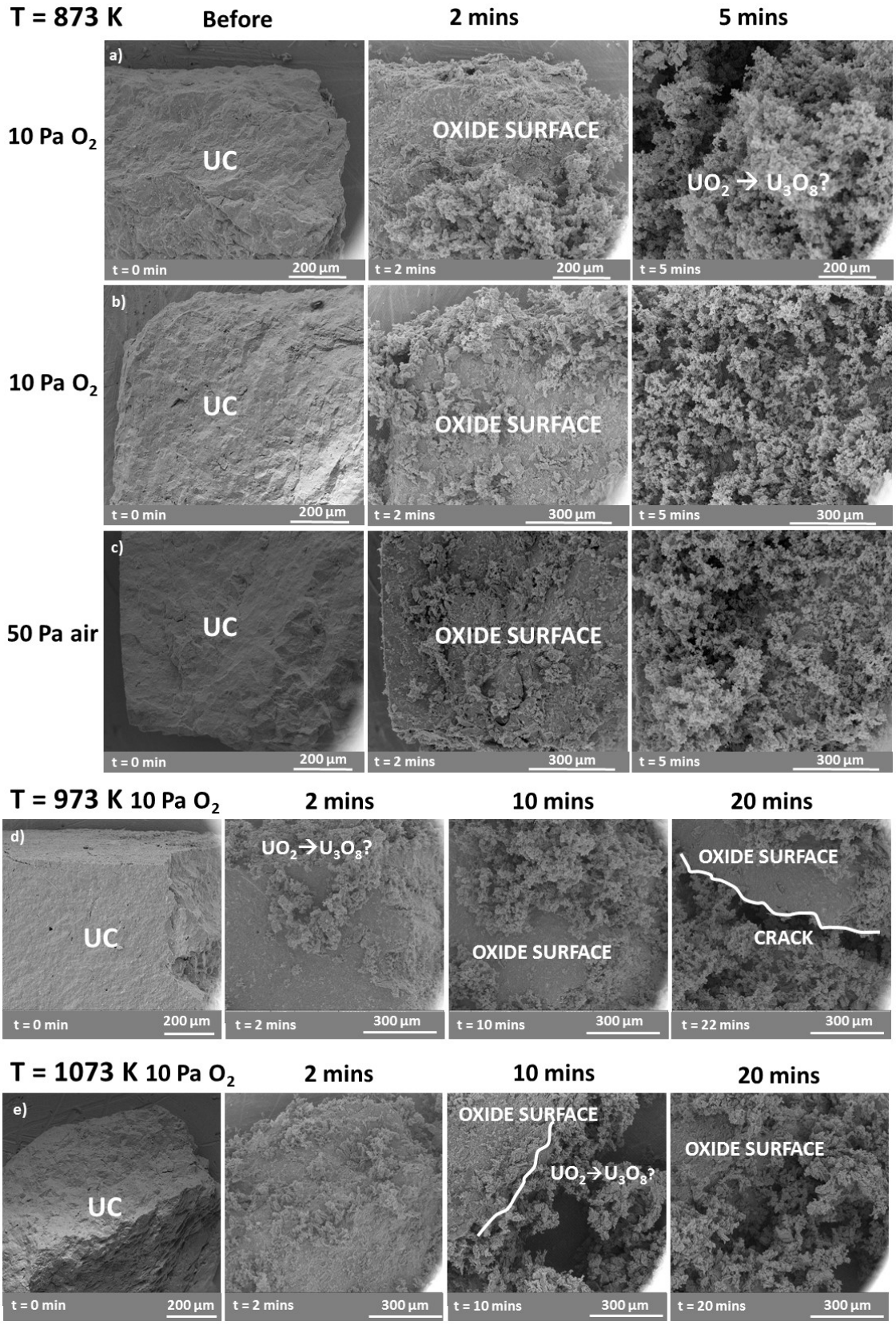

Figure 6 SEIs sequence showing UC fragments oxidation at T= 873 K in a HT-ESEM in 10 Pa O_2 atmosphere (a and b) and 50 Pa air atmosphere (c). Sequence shows three stages: initial sample (before oxidation), 2 minutes

after oxygen insertion, 5 minutes after oxygen insertion. Sequence showing UC fragments oxidation at T=973 K (d) and 1073 K (e) before oxidation and after 2, 10 and 20 minutes of oxygen exposure

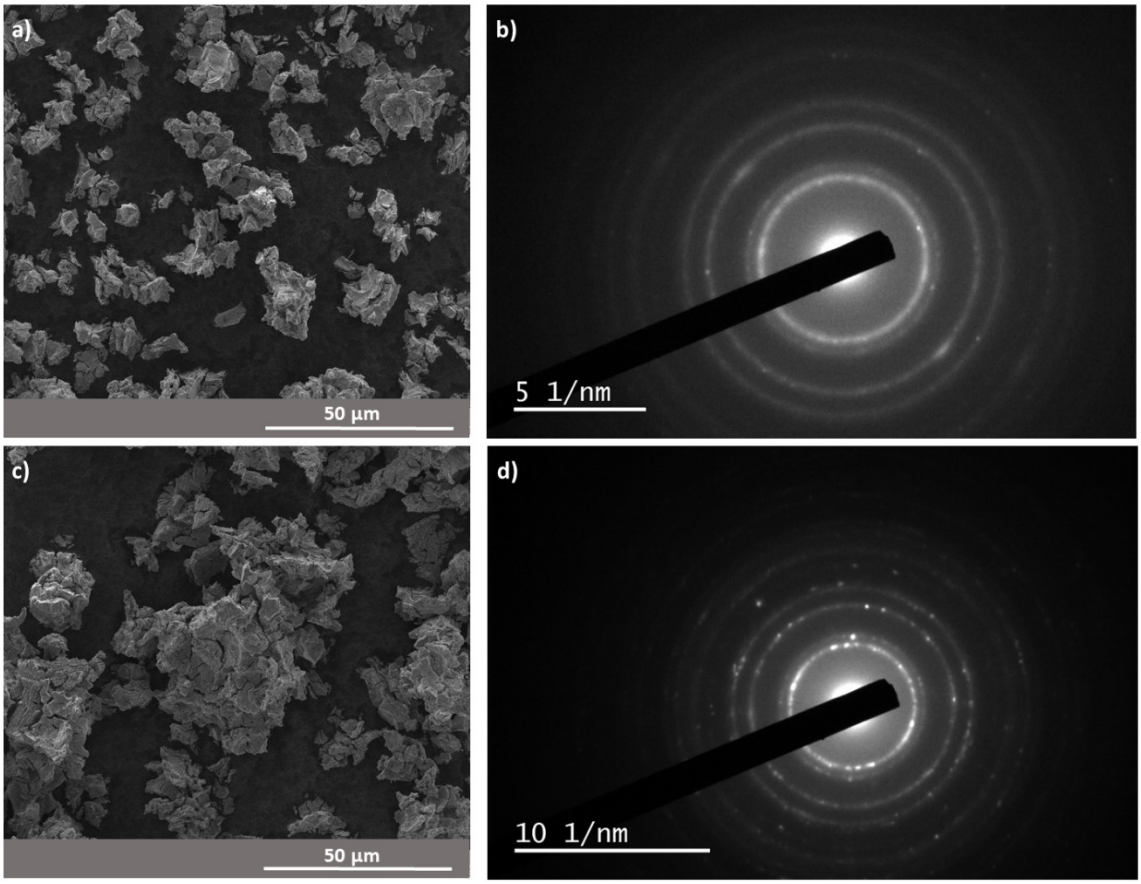

Figure 7 SEIs on the products of oxidations performed *in situ* in a HT-ESEM at 873 K (a) and 973 K (c) in 10 Pa O_2 atmosphere. SADP from the oxide powders: b is related to the oxide produced at 873 K and d to the oxide produced at 973 K.

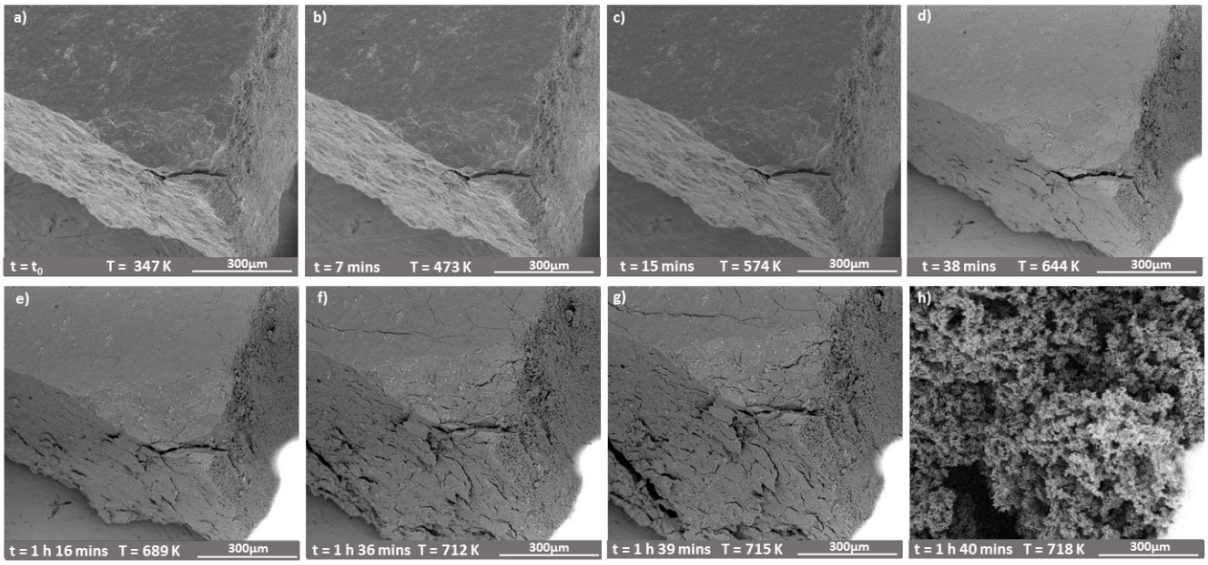

Figure 8 Sequence of SEIs showing a UC sample oxidised *in situ* in a HT-ESEM in a 10 Pa O_2 atmosphere from room temperature to 623 K at 20 K/min and from 623 K to 723 K at 1 K/min

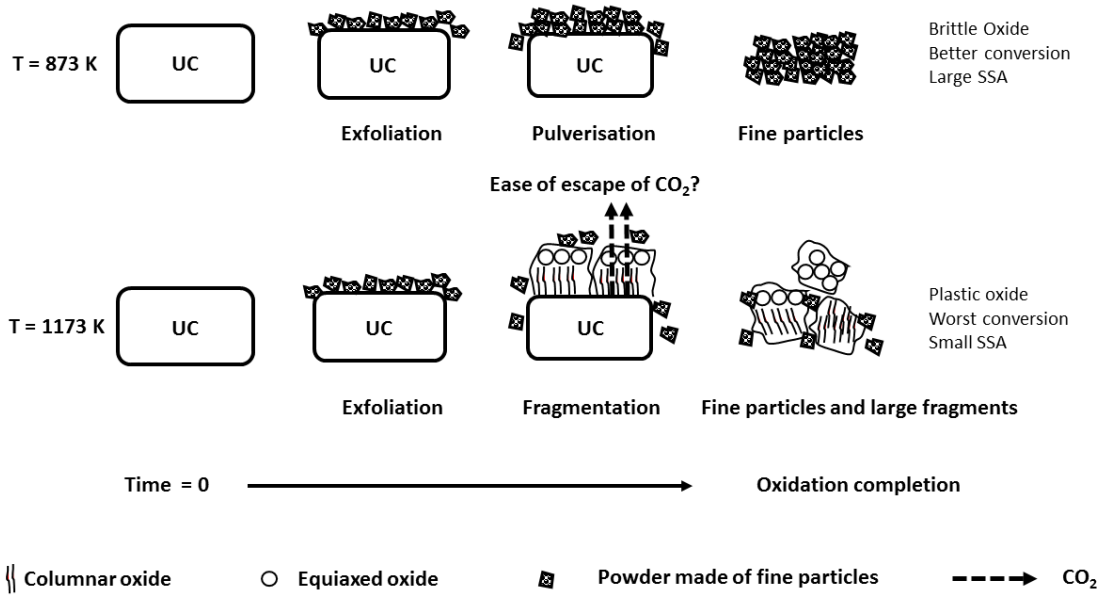

Figure 9 Summary of the mechanism of oxidation of UC from 873 K to 1173 K showing pulverisation and fragmentation processes with temperature.

8.2 List of Tables

Table 1 Masses of Set A and B pellets used for oxidation in air at 873 K and 1173 K for 6 h dwell time.

Sample	Mass (g)	Temperature (K)	Dwell time (h)	Time in the furnace (h)
Set A (P1)	81.54 ± 0.01	1173	6	22
Set B (P2)	5.45 ± 0.01	1173	6	22
Set A (P3)	81.85 ± 0.01	873	6	17.5
Set B (P4)	5.44 ± 0.01	873	6	17.5

Table 2 Dimensions and masses of oxide products (oxide powder and unreacted UC) from Set A and Set B pellets used for oxidation at 873 K and 1173 K for 6 h in air. Oxide conversion, *X*, was calculated on Set A pellets considering the mass of the unreacted UC core after oxidation. Carbon analysis was performed on the oxide layer.

Sample	Dimensions UC core (mm)	Mass (g)	Conversion *X* (%)	Carbon % (w/w)
Set A (P1)	15.6 × 13.4	21.78 ± 0.01 (UC core)	73	0.2
Set B (P2)	N/A	6.11 ± 0.01	100	0.0327 ± 0.0042
Set A (P3)	14.5 × 12.9	19.68 ± 0.01 (UC core)	76	0.47
Set B (P4)	N/A	6.08 ± 0.01	100	0.047

Table 3 Calculated d spacings at room temperature measured on SADP rings from oxide produced at 873 K and 973 K, these were compared with PDF tabulated for UO_2, U_3O_7, U_4O_9. Peak intensity (I) is given within brackets.

d spacing (Å)				
SADP 873 K oxide	**SADP 973 K oxide**	**c-UO_2 PDF 041 1422**[30]	**t-U_3O_7 PDF 015 0004**[32]	**c-U_4O_9 PDF 01 075 0944**[33]
3.21±0.03	3.13±0.01	3.15 (I=100%)	3.14 (I=100%)	3.14 (I=100%)
2.77±0.01	2.72±0.02	2.73 (I=50%)	2.72 (I=30%)	2.72 (I=38%)
1.96±0.01	1.92±0.01	1.93 (I=50%)	1.93 (I=20%)	1.92 (I=44%)
1.68±0.01	1.64±0.01	1.65 (I=45%)	1.65 (I=20%)	1.64 (I=35%)
1.39±0.01	1.39±0.01	1.37 (I=10%)	1.37 (I=5%)	1.36 (I=5.4%)
1.26±0.01	1.23±0.01	1.25 (I=20%)	1.25 (I=10%)	1.25 (I=11.6%)

Table 4 Approximate values of strain and stresses in oxide layer during oxidation of UC to UO_2 and of UO_2 to U_3O_8.

Species	**Z**	**V/Z per metal ($Å^3$)**	**d^* (Å)**	**E (GPa)**	**ν**	**Reaction**	**ε**	**σ (GPa)**	**Ref. (E, ν)**
UC	4	30.45	3.123						
UO_2	4	40.85	3.444	145 220	0.302	UC→UO_2	-0.094	-34.42 -52.22	[45], [53] [54]
U_3O_8	2	55.516	3.815	151	0.36*	UO_2→U_3O_8	-0.097	-52.31	[55], [56]
						UC→U_3O_8	-0.181	-97.61	[55], [56]